Quantification of self-sputtering and implantation during pulsed laser deposition of gold

Cite as: J. Appl. Phys. **104**, 084912 (2008); https://doi.org/10.1063/1.2988145
Submitted: 15 April 2008 . Accepted: 07 August 2008 . Published Online: 30 October 2008

A. Perea, J. Gonzalo, C. Budtz-Jørgensen, G. Epurescu, J. Siegel, C. N. Afonso, and J. García-López

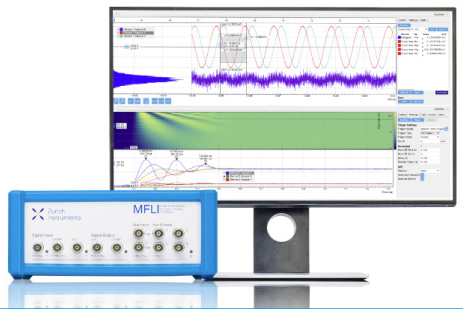

Quantification of self-sputtering and implantation during pulsed laser deposition of gold

A. Perea,[1] J. Gonzalo,[1] C. Budtz-Jørgensen,[1] G. Epurescu,[1,a)] J. Siegel,[1] C. N. Afonso,[1,b)] and J. García-López[2]
[1]*Laser Processing Group, Instituto de Óptica, CSIC, Serrano 121, 28006 Madrid, Spain*
[2]*Centro Nacional de Aceleradores, P. Tecnológico "Cartuja 93," 41092 Sevilla, Spain*

(Received 15 April 2008; accepted 7 August 2008; published online 30 October 2008)

This work reports on the quantification of self-sputtering and implantation occurring during pulsed laser deposition of Au as a function of the laser fluence used to ablate the gold target. The experimental approach includes, on one hand, *in situ* electrical (Langmuir) and optical (two-dimensional imaging) probes for determining, respectively, ion and excited neutral kinetic energy distributions. On the other hand, it includes determination of the density of (i) ions reaching a substrate, and (ii) gold atoms deposited on a substrate as well as of a proportion of atoms that are self-sputtered. The experimental results supported by numerical analysis show that self-sputtering and implantation are both dominated by ions having kinetic energies ≥ 200 eV. They are a fraction 0.60–0.75 of the species arriving to the substrate for ablation laser fluences 2.7–9.0 J cm^{-2}. Self-sputtering yields in the range 0.60–0.86 are determined for the same fluence range. © *2008 American Institute of Physics*. [DOI: 10.1063/1.2988145]

I. INTRODUCTION

Pulsed laser deposition (PLD) has proven to be an attractive technique for producing many materials including metal systems such as alloys,[1] multilayers[2] or nanoparticles.[3] It has successfully been applied to produce metastable alloys[4] or ultrathin films with improved magnetic behavior.[5] It is generally accepted that the special features or improved performance of pulsed laser deposited metal systems relate to their different structure and microstructure when compared to metal systems produced using conventional techniques. The high kinetic energy of species arriving to the substrate is the most widely reported reason for these differences.[1,3,4,6,7] Ion energies higher than 100 eV are typically reported whereas those of neutral atoms are generally considered to be an order of magnitude smaller. However, the presence of species having high kinetic energies is a concern due to effects that can be undesired, such as resputtering or self-sputtering of the deposited species,[3,8] mixing or alloying at the interface,[1,2] subsurface implantation[2,3] or even defect formation.

It is well known that high kinetic energy species bombarding a surface can affect the deposition process.[9] High self-sputtering yields during PLD of gold films have been estimated.[6] Such self-sputtering processes have been quantified for PLD of other metals with yields as high as 0.5 and 1.0 for deposition of Ag (Ref. 8) or Zn (Ref. 10), respectively. To reduce sputtering, the use of low laser fluences (<2 J cm^{-2}) is recommended for Ag and Fe.[8] Results reported on the production of Bi (Ref, 11) and Au (Ref. 3) nanoparticles (NPs) by PLD show that surface nucleation of NPs was unexpectedly reduced for the case of Au and even prevented for the case of Bi when increasing the laser fluence thus confirming the importance of sputtering in these cases. Furthermore, the importance of self-sputtering has been reported during PLD of Au through the observation of a severe distortion of the plasma expansion caused by self-sputtered Au atoms.[12] In addition, ion implantation in the substrate leading to subsurface formation of Bi and Au NPs has been reported for fluences in the range 0.4–5 J cm^{-2} and 2.7–9 J cm^{-2}, respectively,[3,11] the implantation depth scaling with laser fluence. Although both sputtering and implantation have unambiguously been observed in earlier PLD works and related to the high kinetic energy of the species involved, their complete origin is not yet well understood. This is in part due to the lack of detailed information on the actual kinetic energy of the species reaching the substrate in a broad laser fluence range, since average or mean values are typically reported rather than velocity distributions.

The aim of this work is to quantify self-sputtering when producing metal systems by PLD through the correlation of the kinetic energy distributions of both ions and excited neutrals to the areal density of metal species deposited (or self-sputtered) on (from) a substrate. In addition, the implantation will be quantified by comparing the rate of implanted atoms reported in Ref. 3 to the kinetic energy distributions. The study has been performed in a wide fluence interval from near plasma formation threshold up to 9 J cm^{-2}. Gold was chosen for the present study since both effects have been reported to take place during the growth of Au NPs by PLD thus making a very good case study.[3] The experimental approach involves a Langmuir probe (LP) to determine ion kinetic energy distributions and densities, and time-gated optical imaging to determine excited neutral kinetic energy distributions. These parameters are correlated with the areal density of metal atoms deposited on two substrates located in a configuration that allowed quantifying a proportion of self-sputtered to deposited species.

[a)]Present address: National Institute for Lasers, Plasma and Radiation Physics, P.O. Box MG–16, 077125 Magurele-Bucharest, Romania.
[b)]Electronic mail: cnafonso@io.cfmac.csic.es.

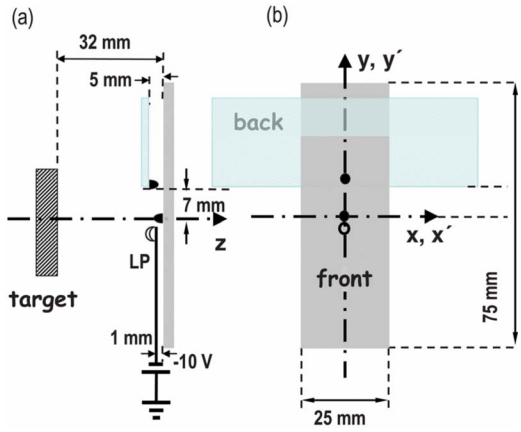

FIG. 1. (Color online) Schematics of the location of the target, back and front substrates and the LP: (a) lateral and (b) front views with respect to substrates. The points at which the number of atoms [(a) ◗, ◖; (b) ●] or ions [(a) ℄; (b) ◯] are measured in the substrates by RBS or LP probe, respectively.

II. EXPERIMENTAL

Laser ablation was performed using an ArF laser ($\lambda=193$ nm, $\tau=20$ ns full width at half maximum, 10 Hz). The laser beam was focused on the surface of a Au (99.99%) target in vacuum ($<10^{-5}$ mbar) at an angle of incidence of 45° and with a fluence ranging from the plasma formation threshold up to 9 J cm^{-2}. The target was continuously rotated except for the LP measurements. The laser fluence was varied using a beam attenuator while keeping constant the laser energy and focusing conditions at the target surface. The fluence was calculated by dividing the energy at the target site by the spot area determined by measuring the ablated area in an aluminum foil located at the target site.

Glass substrates (6×2 cm^2) held at room temperature and located opposite to the target at a distance of 32 mm as seen in Fig. 1 were used for Au deposition. These substrates will be referred to from now on as *front substrates*. In order to determine a proportion of species self-sputtered from this front substrate, a second *back substrate* was located 5 mm from the front substrate toward the target and shifted upwards by 7 mm from the center of the plasma in such a way that it partly covered the front substrate (see Fig. 1). Rutherford backscattering spectrometry (RBS) was used to determine the metal content of the films deposited on both substrates. A 2.0 MeV ^{4}He$^+$ beam was used to probe an elliptical area of ≈2 mm^2. The experimental spectra were analyzed using the SIMNRA simulation code, the error in the determination of the gold content being 2%.

The density and kinetic energy distributions of Au$^+$ ions in the plasma were determined using a LP having a sensitive area of $\approx2.0\pm0.1$ mm^2 placed at 31 mm from the target surface as also shown in Fig. 1. The main error source in the density measurements is provided by the uncertainty in the LP probe dimensions, i.e., 5%. The LP was biased at a voltage of −10 V to ensure that only ions and not electrons were collected, while its rear side was electrically insulated using a teflon sheet. Real time current transients were collected by a Koopman circuit connected to a digital oscilloscope. Two laser pulses separated by 1 s were used: the first one to clean the target surface and the second one for recording the current transient. Whereas the second pulse induces a current transient that contains the broad and long lasting peak typically recorded by LP probes,[13] the first pulse induces in addition a weak and narrow peak at short times. In all cases, the intensity of the broad and long lasting pulse increases sharply as the ablation fluence increases, whereas that of the peak appearing at short times after the first pulse shows no significant changes. The origin of the latter weak peak was explored by varying several conditions and it was found it relates to target contamination (probably related to the limited vacuum conditions) since it disappears after the first laser pulse and reappears after a few seconds. All LP data reported in this work thus correspond to current transients collected from the second pulse acquired from a target point irradiated with pairs of pulses.

The kinetic energy distribution $N(E)$ of Au$^+$ ions has been determined from current transients collected with the LP by first computing the ions flux, $F(t)=I(t)/Se$, where $I(t)$ is the current received in the LP, S is the LP surface, and e is the elemental charge $1.6\ 10^{-19}$ C. Finally, the transformation $N(E)=F(t)|J(E)|$ is used,[14] where $E=0.5m(d/t)^2$, m is the mass of a neutral atom, $d=31$ mm is the position of LP with respect to the target surface, t is the time delay with respect to the laser pulse, and $J(E)=t^3/md^2$ is the Jacobian.

The kinetic energy distribution of excited neutrals has been determined using two-dimensional (2D) imaging (Y-Z plane, Fig. 1) of the expanding plasma using a time-gated intensified change coupled device (ICCD) camera with a 512–512 pixel sensor, an effective pixel size of 24 μm and an analog to digital resolution of 16 bit. Time-gated series of images (field of view: 55×55 mm^2) have been recorded at different delays with respect to the laser pulse, averaging for each delay over 20 consecutive laser shots and using a constant gate width of 100 ns. The delay was varied up to 2000 ns in order to follow the complete plasma expansion process, from plasma formation up to the time the species have reached the substrate. A narrow band pass filter has been used in order to record only the emission corresponding to the 479.3 and 481.2 nm emission lines of excited gold neutrals and the 2D images are similar to those reported elsewhere.[12] The intensity profiles $I(z)$ of these transient excited-neutrals spatial emission distributions are taken along the expansion direction z and converted into kinetic energy distributions using the following method. First, the emission near the target surface (1–2 mm) that corresponds to *bremsstrahlung* is removed from the profiles. The so-corrected spatial distribution profiles are then converted into velocity distributions $\Phi(v)$ by dividing the expansion axis units (z) by the corresponding delay time t at which the image was recorded and normalizing to unit area. These velocity distributions were found to be independent of the delay time for a given laser fluence, as expected for expansion of species in vacuum. This confirms that monitoring the *excited* neutral species provides representative measurements of the overall neutral expansion dynamics. For the following study, a fixed delay time of 2000 ns has been chosen, giving a reasonable compromise between signal intensity and wide

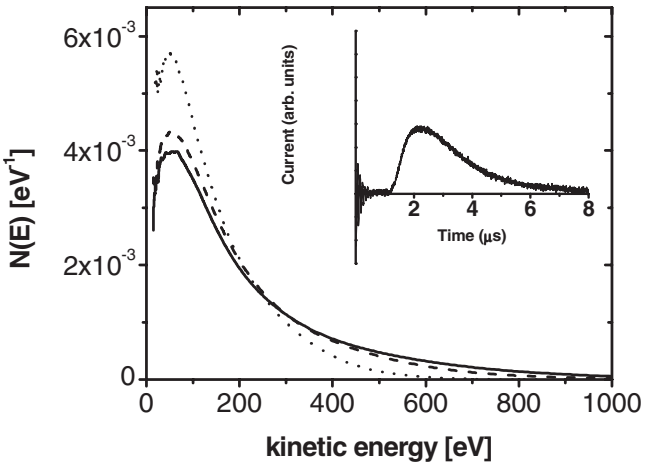

FIG. 2. Kinetic energy distribution of gold ions produced by ablation at 2.3 J cm^{-2} (dotted line), 6.3 J cm^{-2} (dashed line), and 9.0 J cm^{-2} (full line) determined using electric probes. The inset shows a typical current transient.

spatial expansion. The velocity distributions obtained at 2000 ns are finally converted into kinetic energy distributions $N(E)=\Phi(v)|J(E)|$, using the relationship $E=0.5$ mv^2, where m is the mass of a neutral atom and $J(E)=1/\mathrm{mv}$ is the Jacobian.

III. RESULTS

Figure 2 shows kinetic energy distributions of ions determined for three representative laser fluences. All distributions exhibit a maximum at relatively low energy whose position does not depend significantly on fluence, followed by a long tail that extends into high kinetic energy values. The inset in Fig. 2 shows a typical current transient collected after exposing the target to the second pulse. It shows a broad peak whose intensity and width increase with fluence and from which kinetic energy distributions are calculated. The distributions broaden as fluence is increased, all showing kinetic energy values well above 200 eV. Figure 3 shows the kinetic energy distributions of excited neutrals determined from the optical transients for the lowest and highest fluences. It is noticeable that even at the highest fluence, the fraction of species having kinetic energies $\geq$200 eV is very small and the distribution varies little with fluence in the high kinetic range. The inset shows a magnification of the low energy area that evidences that the peak energies are in the range 4–8 eV.

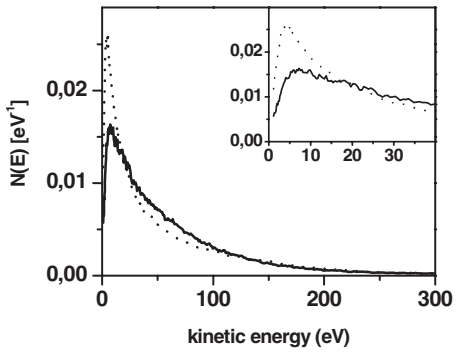

FIG. 3. Kinetic energy distribution of gold neutrals produced by ablation at 2.7 J cm^{-2} (dotted line) and 9.0 J cm^{-2} (full line) determined using optical probes.

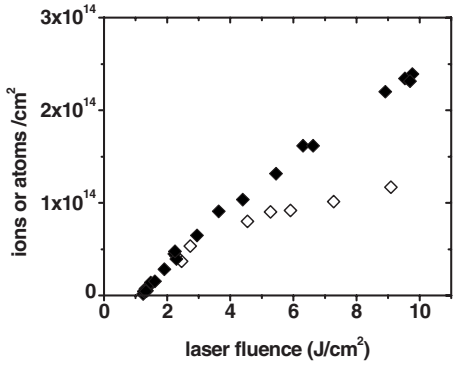

FIG. 4. (♦) Density of ions per pulse measured by the LP $[N_F^a(\mathrm{Au}^+)]$ and (◇) density of atoms deposited per pulse at point $(x,y)=(0,0)$ of the front substrate $[N_F^d(0,0)]$ as a function of fluence. Errors are within symbols.

Figure 4 shows the dependence of the density of ions arriving per pulse at the LP $[N_F^a(\mathrm{Au}^+)]$ as a function of laser fluence. There is a fluence threshold around 1.3 ± 0.1 J cm^{-2} for ions to be detected above which their density increases with fluence. Figure 4 also includes the density of atoms deposited per pulse at the front substrate $[N_F^d(0,0)]$ determined by RBS at point $(x,y)=(0,0)$ (see Fig. 1), that is 1 mm further away from the target than the LP. Since the LP probe signal follows a $1/d^2$ dependence, where d is the target to LP distance, the density of ions at the front substrate and LP position are equal within symbol width. It is seen that $N_F^d(0,0)$ also increases with fluence, the values nearly overlapping with $N_F^a(\mathrm{Au}^+)$ for low fluences. However, they become significantly smaller than $N_F^a(\mathrm{Au}^+)$ for fluences >4.5 J cm^{-2}. It is worth pointing out that whereas LP collects all ions (either single or multiple ionized, excited or ground state), the substrate collects both ions and neutrals. Therefore, if one assumes that all arriving species stick to the substrate, $N_F^d(0,0)$ should be higher than $N_F^a(\mathrm{Au}^+)$ as opposed to what is seen in Fig. 4.

Figure 5 shows the percent of metal atoms deposited on front $N_F^d(0,0)$ substrate per laser pulse with respect to the total number of atoms $[N_F^d(0,0)+N_B^d(0,8)]$ deposited per laser pulse on both front and back substrates as a function of fluence, $N_B^d(0,8)$ being measured at point $(x',y')=(0,8)$ as indicated in Fig. 1. It is seen that the number of atoms deposited on the front substrate (contributing to NPs or film)

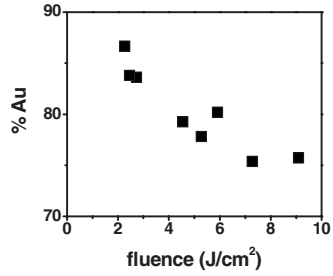

FIG. 5. Percent of metal atoms on (■) front substrates with respect to the total number of atoms collected in both front and back substrates. Errors are within symbols.

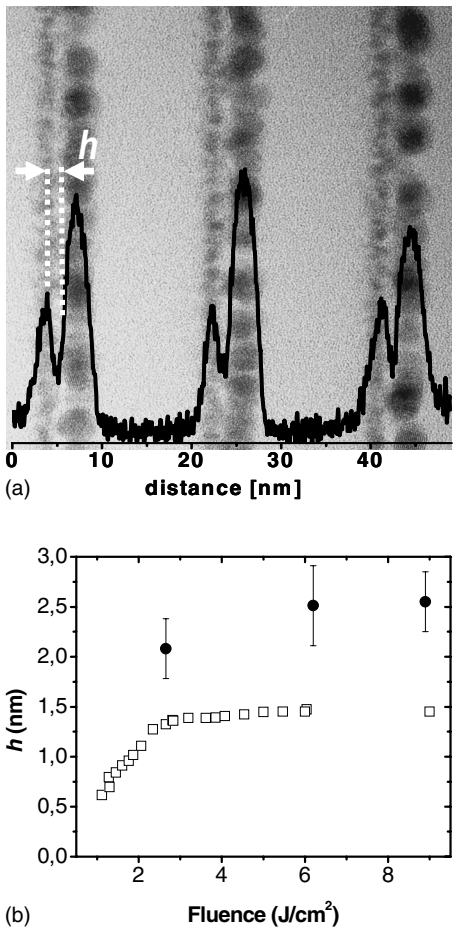

FIG. 6. (a) Cross-section image of Au NPs produced at a fluence of 2.7 J cm^{-2} adapted from Fig. 5 in Ref. 3. The intensity profile overlapped illustrates the procedure used to determine the (●) implanted layer depth $\boldsymbol{h}$ shown in (b) as a function of laser fluence. The implanted layer (□) calculated using the SRIM code and average ion kinetic energy values are also included in (b).

decreases up to 25% as fluence increases. This variation is a consequence of the increase in atoms deposited on the back substrate that accounts for atoms that have been self-sputtered from the front one.

Figure 6(a) shows a cross-section image adapted from Ref. 3 of a sample containing Au NPs embedded in Al_2O_3 host produced by alternate PLD of Au and Al_2O_3 targets. The gold has been ablated at 2.7 J cm^{-2} under similar conditions as in the present experiment. The image shows that even at this low fluence, pairs of NP layers are produced. The first and deepest one contains small NPs (1.4 ± 0.2 nm in diameter) produced by subsurface implantation whereas the second one contains larger NPs produced by surface nucleation.[3] The metal implantation depth $\boldsymbol{h}$ is defined as the depth of the center of the ion distribution inside the material with respect to the surface. In our case, the surface for the implantation process that would be the edge of the large NPs cannot be straightforwardly determined as seen in Fig. 6(a) since these large NPs are not all aligned. In order to estimate this depth, we have recorded the contrast of images through three pairs of consecutive layers as illustrated by the intensity profile also shown in Fig. 6(a). From these profiles, $\boldsymbol{h}$ is calculated as the separation between the two maxima minus the half of the distance between the maximum related to the center of large NPs and the minimum related to the host area between both NPs layers. We have averaged over four different areas of the cross-section images containing each three pairs of layers. The results are plotted in Fig. 6(b) as a function of the laser fluence where it is seen that $\boldsymbol{h}$ is close to 2.0 nm for 2.7 J cm^{-2} and it increases slightly as fluence is increased. The error quoted is the dispersion of the 12 calculated data.

IV. DISCUSSION

According to earlier reports, the emission of the plasma for long distances and delay times is mainly related to excited neutrals since the contribution of excited ions is very weak and disappears soon.[12,15,16] In addition to the ions detected by the LP and the excited neutrals detected by the ICCD, there is a significant fraction of ground neutrals in the plasma that are not detected by any of the probes used in this work. Ground neutrals are expected to behave similarly to excited neutrals or to have even smaller kinetic energies. According to the kinetic energy distributions shown in Figs. 2 and 3, it is clear that only the kinetic energy of ions has a strong dependence on fluence in the high energy range. Therefore, the changes observed when collecting the species on a substrate when fluence is increased must be related to ions.

Ions can thus be considered to dominate the plasma expansion dynamic changes, the higher the fluence the more accurate this assumption becomes. Ions play in addition a significant role in the film growth process,[17] a wide range of ionization fractions (IFs) ranging from 5% to 100% having been reported. In the case of metals, IF is observed to increase sharply with laser fluence[13,17] and for a fixed fluence, it increases with the melting temperature of the metal.[13] Values as high as 0.57[13] or 0.70[18] have been reported for Ag ablated at 2 or 4.5 J cm^{-2}, respectively. Since the melting point for Au is very close to that of Ag, similar IF values are expected. In the present work, IF has been estimated from $N_F^a(\mathrm{Au}^+)$ measured by the LP, $N_F^d(0,0)$, the self-sputtering yield (Y_{SS}) determined using the SRIM2003 software,[21] and the value of the amount of Au atoms that arrives per pulse to the front substrate $N_F^a(\mathrm{Au})$, which has been calculated using the expression[12]

$$N_F^d(0,0) = N_F^a(\mathrm{Au}) + N_F^a(\mathrm{Au}^+) - Y_{SS}N_F^a(\mathrm{Au}^+). \quad (1)$$

It must be noted here that the discussion on the reliability of SRIM2003 software reported elsewhere is not expected to be relevant in our case since the atomic number of the projectile is either equal (self-sputtering) or much higher (implantation) than that of the target.[19] IF is straightforwardly estimated as

$$IF = \frac{N_F^a(\mathrm{Au}^+)}{N_F^a(\mathrm{Au}) + N_F^a(\mathrm{Au}^+)}. \quad (2)$$

The resulting values are all summarized in Table I for two representative extreme fluences. The results are 0.60 and 0.75 for the low (2.7 J cm^{-2}) and high (9.0 J cm^{-2}) fluences, respectively, and are in good agreement with values

TABLE I. IF calculated for two laser fluences using the density of Au^+ ions per pulse arriving to the front substrate $[N_F^a(Au^+)]$, the amount of metal deposited per pulse on point $(x,y)=(0,0)$ of the front substrate $[N_F^d(0,0)]$, the amount of Au atoms arriving per pulse to the front substrate $[N_F^a(Au)]$, and the gold self-sputtering yield (Y_{SS}) calculated using the SRIM2003 software.

Fluence (J cm^{-2})	IF	$N_F^a(Au^+)$ (ions cm^{-2})	$N_F^d(0,0)$ (at. cm^{-2})	$N_F^a(Au)$ (at. cm^{-2})	Y_{ss}
2.7	0.60	0.5×10^{14}	0.5×10^{14}	0.3×10^{14}	0.60
9.0	0.75	2.2×10^{14}	1.0×10^{14}	0.7×10^{14}	0.86

earlier published.[13,18] The high value of IF together with the fact that $N_F^a(Au^+)$ becomes much higher than $N_F^d(0,0)$ for fluences above 2.7 J cm^{-2} as shown in Fig. 4, confirms further that self-sputtering at the front substrate is mainly caused by incident ions.

The importance of self-sputtering on the PLD process of Au is further evidenced by the results presented in Fig. 5. A fraction that lies in the range of 15%–25% of Au species arriving to point $(x,y)=(0,0)$ of the front substrate is self-sputtered and collected at the measuring point of the back substrate $(x',y')=(0,8)$. We have numerically evaluated the extent of self-sputtering for low (2.7 J cm^{-2}) and high (9.0 J cm^{-2}) fluences using the model developed by van de Riet *et al.*[14] with minor modifications. The procedure is described in detail in the Appendix where we have assumed that self-sputtering is caused by ions that have a strongly forward peaked angular distribution of the type $\cos^{19}\theta$, the exponent $n=19$ being taken from Ref. 13. Integrating Eq. (A4), we obtain that the density of species deposited per pulse on the back substrate at the measuring point $N_B^d(0,8)$ to $N_F^d(0,0)$ ratio is 0.32 of the sputtering yield Y_{SS}. Using the values of Y_{SS} included in Table I, the self-sputtered to deposited material ratios are 0.19 and 0.27 at 2.7 and 9.0 J cm^{-2}, respectively. These values are in excellent agreement with the experimental results shown in Fig. 5 thus confirming that the self-sputtering yields of Au are in the range of 0.60–0.86 for the studied fluences.

To quantify the implantation process, average kinetic energies in the range of 80–100 eV determined from the temporal position of the maximum intensity of optical transients were earlier considered.[3] Using this mean value together with a density of 2.95 g cm^{-3} for a-Al_2O_3,[20] and the SRIM2003 software,[21] the calculated implantation depth $\boldsymbol{h}$ of gold in a-Al_2O_3 is shown in Fig. 6(b) where it is seen that it approaches saturation for fluences higher than 3 J cm^{-2}. The experimental values instead increase slightly. In addition, the former values are always lower than the experimental ones and for the highest fluence (9 J cm^{-2}), they become nearly half.

SRIM simulations can be refined taking into account that only a fraction of the arriving species gets implanted. A fraction 0.42 ± 0.01 is estimated from the ratio of metal species in the implanted layer to the total metal deposited reported in Ref. 3. Assuming implantation is caused by energetic species, we have extracted from the distributions in Fig. 2 this fraction of ions having the higher kinetic energies. For a fluence of 9 J cm^{-2}, this fraction corresponds to ions having kinetic energies of $\geq$200 eV. Considering that only these ions get implanted, the calculated implantation depth $\boldsymbol{h}$ lies in the range of 2.1–2.3 nm, which is in excellent agreement with the experimental values shown in Fig. 6(b) within experimental error. We can thus conclude that the species contributing to implantation, and thus to subsurface NPs formation in Ref. 3, are ions having kinetic energies $\geq$200 eV.

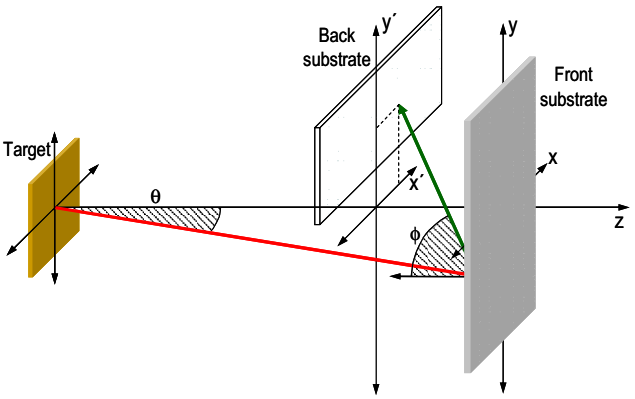

FIG. 7. (Color online) Geometry used to evaluate the self-sputtering.

V. CONCLUSIONS

The analysis of kinetic energy distributions of ions and neutrals determined, respectively, with electrical and optical probes, together with the metal deposited on substrates, allows us to conclude that the ionization fraction of the gold plasma is 0.60–0.75 for laser ablation fluences in the range of 2.7–9.0 J cm^2. We provide experimental evidence supported by numerical analysis that ions are responsible for both self-sputtering at the surface of the substrate and the formation of small Au NPs by implantation below the surface. The comparison of the density of ions at the substrate position with the amount of metal deposited on the back and front substrates allowed us to determine self-sputtering yields of 0.60–0.86 when the gold target is ablated with fluences in the range of 2.7–9.0 J cm^2. It is also shown that gold ions having kinetic energies of $\geq$200 eV are the ones contributing to subsurface NPs production by implantation.

ACKNOWLEDGMENTS

This work was partially supported by Project No. MAT2005-06508-C02-01 of MEC (Spain) and by Project No. HPRN-CT-2002-00328 of EU. We also thank V. Resta (Instituto de Optica, CSIC) for experimental assistance and J.G. Lunney (Trinity College Dublin, Ireland) for helpful discussions.

APPENDIX

The geometry used to evaluate the extent of self-sputtering is illustrated in Fig. 7. The model assumes that the material ejected from the target has an angular distribution of the type $\cos^n\theta$, where θ is the angle with respect to the target normal at the impact point as shown in Fig. 7. According to Ref. 14, the fraction of ejected material that will reach a

point (x,y) of the front substrate placed $d=32$ mm away from the target surface (see also Fig. 1) will be given by

$$N_F^a(x,y) = \frac{(n+1)}{2\pi} N_t \frac{\cos^n \theta}{(d^2+x^2+y^2)}, \tag{A1}$$

where N_t is the total number of species ejected from the target. The amount of metal deposited per pulse at point (x,y) of the front substrate is given by $N_F^d(x,y) = (1-Y_{SS})N_F^a(x,y)$, where Y_{SS} is the self-sputtering yield. The amount N_F^d experimentally measured at (0,0) is

$$N_F^d(0,0) = (1-Y_{SS})\frac{(n+1)}{2\pi}\frac{N_t}{d^2}. \tag{A2}$$

Accordingly, the fraction of self-sputtered atoms will be $Y_{SS}N_F^a(x,y)$. Assuming the angular distribution of the self-sputtered material is of cos ϕ type,[22] the amount of metal deposited at a point (x',y') of the back substrate will be given by

$$N_B^d(x',y') = \frac{Y_{SS}}{\pi}\int\int N_F^a(x,y) \times \frac{\cos^2 \phi}{[d_{FB}^2+(x-x')^2+(y-y')^2]} dxdy, \tag{A3}$$

where d_{FB} is the distance between the front and back substrates [Figs. 1(a) and 7] and ϕ is the angle with respect to the front substrate normal as indicated in Fig. 7. We neglect secondary self-sputtering from the back substrate due to the reduced kinetic energies ($\leq$30 eV) of the species reaching the back substrate.[12] In the present work we have measured the material deposited at point (0, 8) of the back substrate and thus we must define the integration limits along the plane xy of the front substrate to evaluate numerically Eq. (A3). The front-back substrates geometry and substrate dimensions are shown in Fig. 1. Integration limits along x-axis are given by the front substrate dimensions: −12.5 to 12.5 mm, while in the case of the y-axis, they are given by the position of the back substrate and the dimensions of the front substrate, 9 to −37 mm. We choose 9 mm instead of 7 mm to take into account the observed deposition beyond the region defined by the back substrate. The expression to be integrated can then be expressed as

$$N_B^d(0,8) = \frac{Y_{SS}}{2\pi^2}(n+1)N_t d^{n+1} d_{FB}^2 \int_{-12.5}^{12.5} dx \int_{-37}^{9} \times \frac{dy}{(d^2+x^2+y^2)^{(n+3)/2}[d_{FB}^2+x^2+(8-y')^2]^2}. \tag{A4}$$

[1] H. L. Meyerheim, V. Stepanyuk, A. L. Klavsyuk, E. Soyka, and J. Kirschner, Phys. Rev. B **72**, 113403 (2005).
[2] R. Gupta, M. Weisheit, H.-U. Krebs, and P. Schaaf, Phys. Rev. B **67**, 075402 (2003).
[3] J. Gonzalo, A. Perea, D. Babonneau, C. N. Afonso, N. Beer, J. P. Barnes, A. K. Petford-Long, D. E. Hole, and P. D. Townsend, Phys. Rev. B **71**, 125420 (2005).
[4] S. Kahl and H.-U. Krebs, Phys. Rev. B **63**, 172103 (2001).
[5] J. Shen, P. Ohresser, C. V. Mohan, M. Klaua, J. Barthel, and J. Kirschner, Phys. Rev. Lett. **80**, 1980 (1998).
[6] A. Zenkevitch, J. Chevallier, and I. Khabelashvili, Thin Solid Films **311**, 119 (1997).
[7] E. Irissou, B. Le Drogoff, M. Chaker, and D. Guay, Appl. Phys. Lett. **80**, 1716 (2002).
[8] K. Sturm and H.-U. Krebs, J. Appl. Phys. **90**, 1061 (2001), and references therein.
[9] P. Sigmund, Nucl. Instrum. Methods Phys. Res. B **27**, 1 (1987).
[10] J. G. Hidalgo, R. Serna, E. Haro-Poniatowski, and C. N. Afonso, Appl. Phys. A: Mater. Sci. Process. **79**, 915 (2004).
[11] A. Suarez-Garcia, J-P. Barnes, R. Serna, A. K. Petford-Long, C. N. Afonso, and D. Hole, MRS Symposia Proceedings No. 780 (Materials Research Society, Warrendale, PA, 2003), p. Y1.2.1.
[12] J. Gonzalo, J. Siegel, A. Perea, D. Puerto, V. Resta, M. Galvan-Sosa, and C. N. Afonso, Phys. Rev. B **76**, 035435 (2007).
[13] B. Thestrup, B. Toftmann, J. Schou, B. Dogget, and J. G. Lunney, Appl. Surf. Sci. **197–198**, 175 (2002).
[14] E. van de Riet, J. C. S. Kools, and J. Dieleman, J. Appl. Phys. **73**, 8290 (1993).
[15] E. Irissou, B. Le Drogoff, M. Chaker, and D. Guay, J. Appl. Phys. **94**, 4796 (2003).
[16] J. W. Elam and D. H. Levy, Appl. Phys. Lett. **81**, 539 (1997).
[17] R. W. Dreyfus, J. Appl. Phys. **69**, 1721 (1991).
[18] S. Fähler, K. Sturm, and H.-U. Krebs, Appl. Phys. Lett. **75**, 3766 (1999).
[19] K. Wittmaack, J. Appl. Phys. **96**, 2632 (2004).
[20] R. Serna, J. C. G. de Sande, J. M. Ballesteros, and C. N. Afonso, J. Appl. Phys. **84**, 4509 (1998).
[21] J. F. Ziegler, Nucl. Instrum. Methods Phys. Res. B **219-220**, 1027 (2004).
[22] J. Cook, Thin Solid Films **338**, 81 (1999).